



Study of Proton-Exchange Membrane Fuel Cell Degradation and its Counter Strategies: Flooding/drying, Cold Start and Carbon Monoxide Poisoning

Fatima Haidar^{1*} , Divyesh Arora¹ , Adrien Soloy¹ , and Thomas Bartoli¹ 

¹ Capgemini Engineering, Research & Innovation Direction, 12 rue de la Verrerie, 92190, Meudon, France

Abstract

In the context of advancing automotive fleet electrification dynamics, the development of hybrid electric vehicles (HEV) and electric vehicles (EV) serves as a pivotal strategy to mitigate CO₂ emissions and promote decarbonization in the transportation sector. While Battery Electric Vehicles (BEV) are prevalent, Fuel Cell Electric Vehicles (FCEV) are gaining traction as a compelling alternative for heavy mobility, particularly Light Commercial Vehicles (LCV) and trucks where relying solely on batteries may not be feasible. Ensuring the efficiency of FCEVs necessitates a profound understanding and control of fuel cell operational conditions. However, concerns persist regarding fuel cell durability due to specific aging phenomena leading to performance decay after operational cycles. The objective of this study is to build a model to accurately characterize and control the fuel cell within a FCEV, by simulating its behavior during cycling and by dealing with common ageing issues like flooding, cold start, and carbon monoxide poisoning. The model described in this study allows not only to simulate the cathode, the anode, and the fuel cell membrane, but it also proposes strategies to handle the water management at the membrane, deal with cold starts, counter poisoning and, in the end, enhance the fuel cell performance and lifespan.

Keywords: Cold start; Carbon monoxide poisoning; Degradation drying; Electric vehicle (EV); Flooding; Fuel cell (FC); Hybrid vehicle (HV); Matlab-Simulink; Proton Exchange Membrane Fuel Cell (PEMFC).

To cite this paper: Haidar, F., Arora, D., Soloy, A., Bartoli, T. Study of Proton-Exchange Membrane Fuel Cell Degradation and its Counter Strategies: Flooding/drying, Cold Start and Carbon Monoxide Poisoning. International Journal of Automotive Science and Technology. 2024; 8 (1): 96-109. <http://dx.doi.org/10.29228/ijastech.1389241>

1. Introduction

Energy and environmental issues currently represent a major concern at the international level. The world population growth and increasing industrial activity have led to an explosion in energy needs. The use of fossil resources is responsible for a major part of greenhouse gases emissions in the atmosphere, causing climate change. Besides the impact on the environment, fossil fuel reserves are limited and may not meet future energy needs.

Among all the sectors incriminated in these environmental problems, the automotive sector is regularly cited. Indeed, the transportation sector accounts for more than 29% of global fossil-fuel energy consumption. In the last past years, technological advances regarding engines have made them less fuel-consuming and less pollutant, in accordance with the new standards established to limit the pollution coming from the vehicles (for example EURO 4, EURO 5, and EURO 6d) [1]. However, those advances are offset by the increasing number of vehicles in circulation.

To comply with those regulations and decarbonize the transportation sector, the development of Hybrid Electric Vehicles (HEV) and Electric Vehicles (EV) is necessary. EVs are a very promising solution as they consist of a zero-emission mobility, with a high energy efficiency throughout the supply chain. Battery Electric Vehicles (BEVs) are already well-developed by automakers and can already be commonly found on our roads today. However, batteries have well-known limitations in terms of autonomy, due to

their limited gravimetric and volumetric energy densities. To overcome those limitations, research is now more and more focused on Electric Vehicles containing a fuel cell, or Fuel Cell Electric Vehicles (FCEVs), as they are a good alternative to BEVs for heavy mobility such as Light Commercial Vehicles (LCV) and trucks. A FC is an electrochemical device producing electricity from hydrogen and oxygen, with the aid of electrocatalysts. Among the different fuel cell technologies currently investigated, the Proton Exchange Membrane Fuel Cell (PEMFC) is considered the most mature and viable [2]. The hydrogen needed for the fuel cells can be produced from renewable resources, reducing even more the environmental impact of the use of this kind of technology. The efficiency of those systems can reach 65% when operating on hydrogen, with water being the only by-product. The PEMFC technology has reached a mature technology level and car manufacturers such as Toyota, Honda, and Hyundai have already started selling and leasing their FCEV models with yearly updates in various regions, depending on the available infrastructures (H₂ production stations, H₂ Refueling Stations (HRS), ...)[3]. Even though the working principle of PEMFCs is well mastered, different ageing phenomena are responsible for the degradation of the FC performances.

Research Article

History

Received 10.11.2023
Revised 13.02.2024
Accepted 20.02.2024

Contact

* Corresponding author
Fatima Haidar
Fatima.haidar@capgemini.com
Address: Capgemini Engineering, Research & Innovation Direction, 12 rue de la Verrerie, 92100, Meudon, France

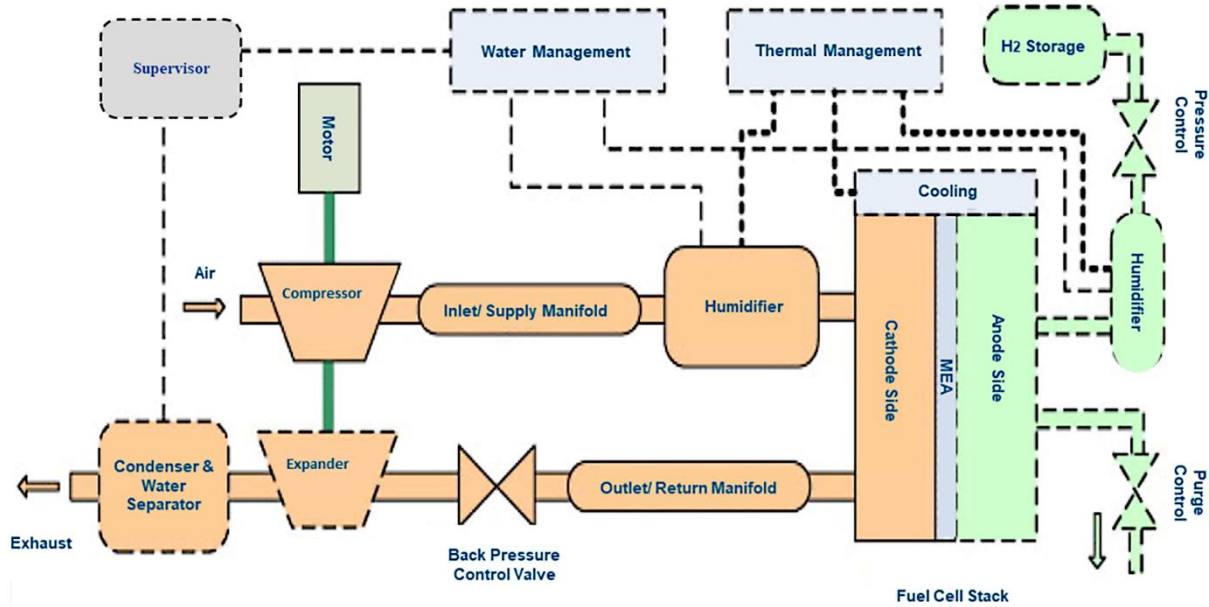


Fig. 1. Illustration of the interconnections between the fuel cell core and its auxiliaries.

The most common ageing issues are the flooding or drying of the membrane, the cold start of the FC and the carbon monoxide poisoning of the catalyst and electrode assembly.

The primary aim of this research is to develop a precise model for characterizing and regulating the fuel cell in a Fuel Cell Electric Vehicle (FCEV). The paper provides a detailed description of the methodology employed in constructing this model using Matlab-Simulink software. The model outlined in this study enables the simulation of the cathode, anode, and fuel cell membrane, with their parameters serving as inputs for the model. It can simulate the electrical behavior of the fuel cell based on its characteristics. Additionally, the model suggests strategies for managing water at the membrane, addressing cold starts, and mitigating carbon monoxide poisoning, thereby improving the fuel cell's performance and longevity.

While the ultimate objective is to integrate this fuel cell model into a comprehensive FCEV model for realistic conditions such as Worldwide harmonized Light vehicles Test Cycles (WLTC), this aspect will not be covered in this paper. The focus here is on presenting the content and the methodology employed in constructing the fuel cell model.

2. Methodology

2.1. Proton-exchange membrane fuel cell (PEMFC) system

Operation of the PEMFC system requires at least five subsystems: a hydrogen source, an oxygen or air source, a system to evacuate residues or reaction products, a thermal management system to maintain the FC at the required temperature, and a power supply. The entire FC system device, with its components and individual circuits, is shown in Figure 1.

The different subsystems of a FC system are:

- The Hydrogen circuit (closed circuit):

It supplies the anode with hydrogen gas. The hydrogen that remains unconsumed at the outlet of the FC can be reinjected at its inlet via a recirculation pump. It is generally composed of a high-pressure tank and two decompression stages to reduce the hydrogen pressure to a suitable level for the FC.

- The air circuit (open circuit):

Generally, to supply the FC with oxygen, a compressor brings air to the cathode. This is the most important lever to control and optimize the performance of the PEMFC. The compressor consumes energy but also allows an improvement of the PEMFC efficiency.

- The cooling circuits:

It is an essential part of the FC system. The heat produced by the FC can represent more than 50% of the power losses for high currents. The heat produced requires the use of heat exchangers to regulate the system temperature. This represents an important technical constraint.

- The water circuit:

The incoming gases (air and hydrogen) enter via the water circuit while humidifying the membrane. Humidification of the membrane is essential to guarantee the electrons transfer and limit the deterioration of the membrane.

In addition to these circuits, it is also necessary to add the equipment needed to ensure proper operation of the system, in particular flow, pressure, and temperature sensors [1]. In this project, the Matlab-Simulink software is used to model the FC system. The modelled FC system, with the different blocks interconnected to each other representing the different parts of the fuel cell and its auxiliary systems, is shown in Figure 2. The numerous interactions between the different components complicates the management of

the FC parameters.

2.2. Advantages and problems associated with the fuel cell systems

2.2.1. Advantages

The main advantages of the PEMFC systems are:

- i. The high energy efficiency. It varies between 30% and 70%, depending on the FC type [4]. In transport applications for example, these efficiencies change from 38% (using methanol reforming) to 50% (using pure hydrogen). The efficiency of the Hybrid Fuel Cell Vehicle (HFCV) is 2 times higher than that of the gasoline-powered vehicle [4].
- ii. The low or zero GHG emissions. PEMFC, using pure hydrogen as a fuel, produces only electricity, water, and heat. In comparison, direct methanol fuel cells (DMFC) produce small amounts of GHG, such as CO₂, CH₄ and CO, that are harmful for the environment.
- iii. The size of the stack according to the required power. The number of cells in series or in parallel can be adapted to meet the power requirements of a given application.
- iv. There are no mechanical wear problems as there are no moving parts in FC [4–7].

2.2.2 Drawbacks

The main drawbacks of the PEMFC systems are:

- i. The high cost of manufacturing of the system due to the presence of a significant amount of precious metals for the catalyst (i.e., Platinum).
- ii. The lack of hydrogen recharging infrastructure, limiting the sales of FC-based vehicles.
- iii. Other auxiliary modules, such as the air compressor, the cooling system, etc., are needed for the integration of a FC module in a traction system. These auxiliaries can represent up to 60% of the mass and volume of the system and an energy expenditure of around 30% [1].
- iv. Water management, necessary to hydrate the membrane, may cause a flooding of the system, hindering the FC operation.

2.3 The fuel cell operating issues

The performance degradation of the FC is closely related to many factors, which leads to an early aging and/or shutdown of the system. Those factors include [8]:

- i. The flooding of the cell. Poor water management can lead to an accumulation of liquid water at the critical parts of the cell and thus to the flooding of the membrane and electrodes. This will prevent access and distribution of reactants throughout the cell [9].

- ii. The membrane drying. The membrane always requires a good hydration rate to allow proper proton diffusion. Otherwise, its resistivity will increase, leading to important energy losses and decreased performance, which may even lead to the destruction of the FC [10].
- iii. The poisoning of the membrane and electrode assembly. The platinum present in the active layers tend to absorb many atmospheric pollutants (H₂S, CO, SO₂, NO_x). The active surface area of the catalyst decreases, and the chemical kinetics of the FC is lowered [9,11].
- iv. The destruction of the catalyst. The agglomeration or dissolution and recrystallization of the catalyst in the membrane leads to a decrease of the active surface of the membrane and the electrodes, causing irreversible performance degradation [9,11].
- v. The destruction of the catalyst support. The oxidation potential of the carbon support is very close to the oxygen reduction potential. As a consequence, oxygen may react with the carbon support leaving the platinum unusable and resulting in a severe loss of FC performance [9].
- vi. The air compressor failure. In case of mechanical failure of the air compressor system, chemical reactions will be lowered which may cause a shutdown of the system.
- vii. The cooling system failure. A failure of the cooling system may lead to an important increase of the FC temperature, causing the destruction of the materials constituting the membrane and the electrodes.
- viii. The hydrogen leakage during storage or operation of the FC. In case of hydrogen leakage, there is an important risk of fire or explosion of the vehicle.
- ix. Impurities in the hydrogen used. Metal ions are impurities that can be found in the hydrogen. These pollutants are usually superimposed on the membrane causing a voltage drop in the FC.
- x. A large pressure difference between anode and cathode. This may create micro-holes on the membrane that will accelerate the ageing of the FC.
- xi. A leakage of carbon monoxide (CO), carbon dioxide (CO₂) or methanol (CH₃OH) during reforming. These gas leakages may be responsible for a risk of asphyxiation if the vehicle is in a confined space. Some of these problems are discussed in detail below with a proposal of strategies adopted to counter them.

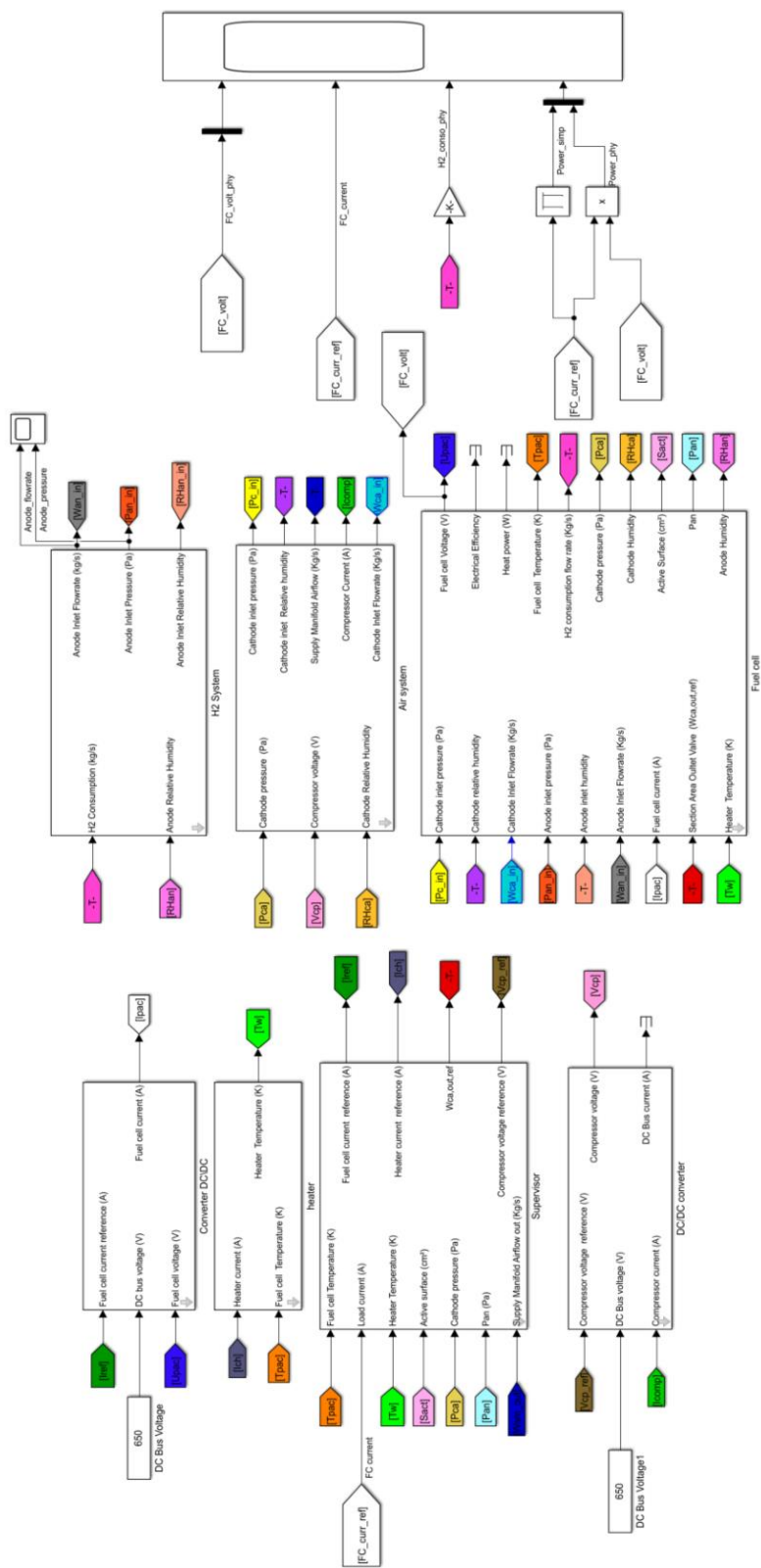


Fig. 2. Final model of the fuel cell system on Matlab-Simulink.

2.4. Problem of water management (flooding and drying) and its control strategy

In a FC system, water management is of crucial importance to maintain the system's performance and increase its lifetime. The membrane must sufficiently be hydrated to keep a good proton conductivity. However, excessive water may accumulate, causing water flooding and thus hindering the transport of oxygen by blocking the pores in the porous cathode catalyst layer (CCL) and the gas diffusion layer (GDL), covering up active sites in the catalyst layer and plugging the gas transport channels in the flow field, resulting in increased resistance to proton transport [12]. The ionic conductivity of the proton-conducting membrane is strongly dependent on its level of humidification, or water content, with high ionic conductivities obtained at maximum humidification. When the water removal rate exceeds the water generation rate, membrane dehydration occurs, which can result in performance degradation due to significant ohmic losses within the cell [12]. An insufficient quantity of water limits the ionic conductivity of the membrane and can lead to its degradation. It is therefore important to control the amount of water in the membrane to protect the FC from various degradations. The physical model that describes the water flow in the FC is defined in several publications [13–16]. The different water flows into and out of the FC are summarized in Figure 3 [17].

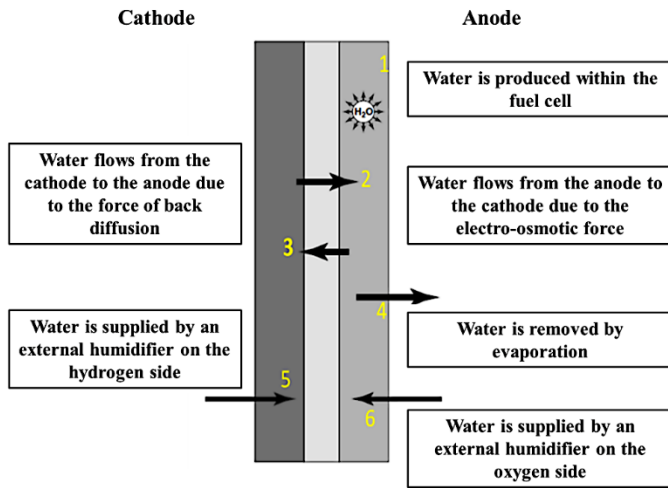


Fig. 3. Representation of the different water flows involved in the PEMFC.

In a FC, two counter phenomena contributing to the hydration of the membrane are usually observed.

- i. Electro-osmosis. This phenomenon occurs when H^+ ions carry water molecules with them through the membrane to the cathode. The electric field created by the FC leads to a movement of free charges, and due to the polarized bond formed between H^+ ions and water, the water molecules are carried along. This phenomenon tends to dry out the membrane on the anode side, especially at high current flow conditions where electro-osmosis becomes important.

- ii. Back-diffusion. When the concentration of water in the cathode exceeds that of the anode, water diffusion begins to occur. This diffusion increases with current density. However, it remains limited by the reduction reaction rate in the cathode because the oxidation reaction in the anode is faster than the reduction in the cathode, and, therefore, back-diffusion can no longer compensate for electro-osmosis.

2.4.1. Membrane hydration model

The model of the membrane represents all the water transport phenomena taking place in the membrane. It gives an idea of the relative humidity, as well as the water content. In this model, the circulation of water through the membrane and its resulting effects, namely the electro-osmotic force and the back-diffusion force are modelled. The evolution of the internal resistance of the membrane obtained by simulation as a function of the relative humidity is shown in Figure 4. When the relative humidity increases from 0 to 100 %, the resistance of the membrane decreases from 0.012 to 0.010 Ω .

Thus, it is shown that relative humidity is important to maintain the low resistance of the membrane. However, it cannot be too humid, or it will cause flooding.

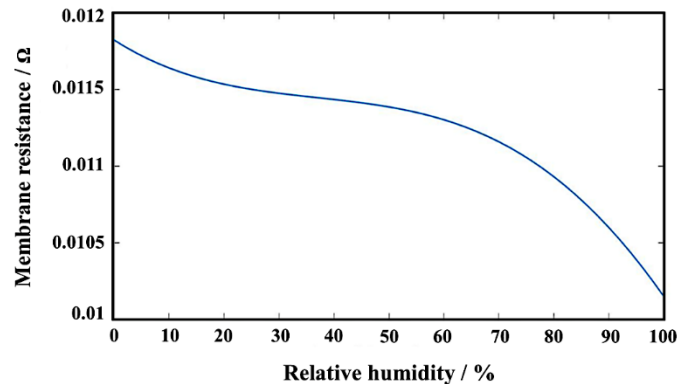


Fig. 4. Evolution of the membrane resistance depending on the relative humidity obtained by simulation.

The flow rate of water through the membrane is obtained using the following equation Eq. (1):

$$W_{v,membr} = N_{v,membr} M_{H_2O} A_{fc} N_{fc} \quad (1)$$

Where A_{fc} is the active surface of the membrane, N_{fc} is the number of cells and $N_{v,membr}$ is the result of the two opposite flow rates (electro-osmotic and back-diffusion). This term is defined by Eq. (2):

$$N_{v,membr} = n_d \frac{i}{F} - D_w \frac{(C_{v,ca} - C_{v,an})}{t_m} \quad (2)$$

Where n_d , i , D_w , $C_{v,ca}$, $C_{v,an}$ are the electro-osmotic coefficient, the current density ($A.cm^{-2}$), the back-diffusion coefficient, the water concentration in the cathode and the water concentration in the

anode, respectively.

The first term $n_d \frac{i}{F}$ represents the electro-osmotic flow rate and the second term the "back-diffusion" flow rate.

The electro-osmotic coefficient n_d is calculated as follows in Eq. (3) [18]:

$$n_d = 0.0029l_m^2 + 0.05l_m - 3.4 \times 10^{-19} \quad (3)$$

Where l_m is the average moisture content.

The back-diffusion coefficient is calculated thanks to the diffusivity coefficient D_l as follows in Eq. (4) [18]:

$$D_w = D_l \exp\left(2416 \left(\frac{1}{303} - \frac{1}{T_{fc}}\right) D_l\right) \quad (4)$$

$$= \begin{cases} 10^{-6}, l_m < 2 \\ 10^{-6}(1 + 2(l_m - 2)), 2 \leq l_m \leq 3 \\ 10^{-6}(3 - 1.67(l_m - 3)), 3 < l_m < 4.5 \\ 1.25 \times 10^{-6}, l_m \geq 4.5 \end{cases}$$

The water concentrations in the anode and the cathode are calculated from the following Eq. (5) and Eq. (6) respectively:

$$C_{v,an} = \frac{r_{m,dry}}{M_{m,dry}} l_{an} \quad (5)$$

$$C_{v,ca} = \frac{r_{m,dry}}{M_{m,dry}} l_{ca} \quad (6)$$

Where $r_{m,dry}$, $M_{m,dry}$, l_{an} , l_{ca} are the dry membrane density ($\text{kg}\cdot\text{cm}^{-3}$), the dry membrane molar equivalent mass ($\text{kg}\cdot\text{mol}^{-1}$), the anode water content and the cathode water content respectively. The different water contents are calculated from the anodic and cathodic activities a by the following relationship Eq. (7):

$$l = \begin{cases} 0a \leq 0 \\ 0.043 + 17.81a - 39.85a^2 + 36a^3 \\ 0 \leq a \leq 1 \\ 14 + 1.4(a - 1)1 < a \leq 3 \\ 16a > 3 \end{cases} \quad (7)$$

For an ideal gas, the activity is equal to its relative humidity.

2.4.2. Problem statement

To highlight the problem related to relative humidity (RH), a simulation was carried out using the previous model without relative humidity control. The FC is simulated for a current ramp from 0 to 300 A ($5 \text{ A}\cdot\text{s}^{-1}$). The evolution of relative humidity obtained for the cathode ($\text{RH}_{\text{cathode}}$) and the anode (RH_{anode}) as a function of time are shown in Figure 5a and Figure 5b respectively. The amount of water generated as a function of time is shown in Figure 6. It is shown in Figure 5a that for low currents, the relative humidity on the cathode side is less than 1 and therefore, there is no water condensation. As the current increases and the generated water flow increases (Figure 6), the amount of water produced in the cathode becomes difficult to evacuate and, therefore, the relative

humidity on the cathode side increases up to values larger than 1, resulting in the flooding of the membrane.

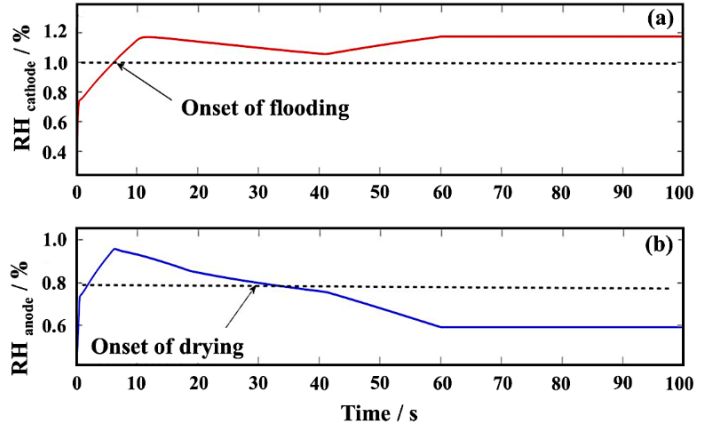


Fig. 5. (a): Relative humidity in the cathode (a) and in the anode (b) for a current ramp from 0 to 300 A obtained by simulation.

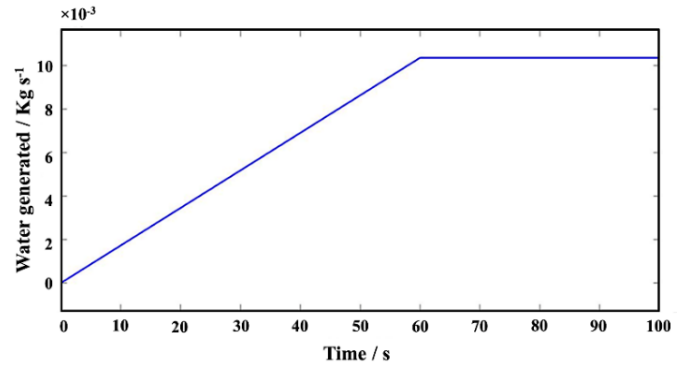


Fig. 6. Water generated by the chemical reaction obtained by simulation.

However, on the anode side (Figure 5b), the phenomenon of electro-osmosis becomes quite important when high currents are required. Then, the H^+ ions drain more water towards the cathode, causing a decrease in the relative humidity down to values lower than 0.8, and leading to the drying of the membrane.

2.4.3. Strategy adopted

A solution to solve the problem previously mentioned is the regulation of the relative humidity of the gases at the anode and cathode, allowing a better management of the quantity of water to be evacuated.

The modelling of the cooler, used to cool the air coming from the compressor, is performed. Then, the modelling of the humidifier to regulate the relative humidity on both sides of the membrane is performed. The control strategy performed in that simulation is illustrated in the scheme in Figure 7.

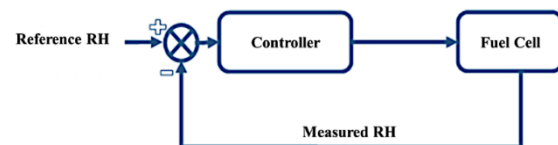


Fig. 7. Control strategy.

2.5. Model of cooler and humidifier

The designs of the cooler and the air system humidifier are based on the mass conservation law [19].

2.5.1. Model of the cooler

The relative humidity of the cooler is calculated by Eq. (8):

$$\phi_{cl} = \frac{p_{sm}\phi_{atm}p_{sat}(T_{atm})}{p_{atm}p_{sat}(T_{cl})} \quad (8)$$

Where ϕ_{atm} , p_{atm} , p_{sm} , $p_{sat}(T_{atm})$, $p_{sat}(T_{cl})$ are the relative humidity of the atmosphere (assumed as 0.5), the atmospheric pressure, the supply manifold pressure and the saturation vapor pressure at ambient temperature and at the cooler temperature respectively.

The outflow of the cooler W_{cl} is considered equal to the air-flow out of the supply manifold W_{sm} , as shown in the following Eq. (9):

$$W_{cl} = W_{sm} \quad (9)$$

2.5.2. Model of the humidifier

The output of the humidifier is obtained from the following Eq. (10) and Eq. (11):

$$W_{hm} = W_{a,cl} + W_{v,hm} \quad (10)$$

Where $W_{a,cl}$ is the air flow rate of the cooler and $W_{v,hm}$ is the vapor flow rate of the humidifier. The output flow of the humidifier W_{hm} corresponds to the input flow of the cathode $W_{ca,in}$, which gives the following Eq. (11):

$$W_{ca,in} = W_{hm} \quad (11)$$

The vapor flow rate in the humidifier is the sum of the vapor flow rate of the cooler $W_{v,cl}$ and the injected vapor flow rate $W_{v,inj}$, which gives the following Eq. (12):

$$W_{v,hm} = W_{v,cl} + W_{v,inj} \quad (12)$$

i. At the cathode

The flow rate to be injected is determined by a PID controller, which regulates the relative humidity of the cathode. The air and vapor flow rates of the cooler ($W_{a,cl}$ and $W_{v,cl}$ respectively) are calculated as follows in Eq. (13), Eq. (14) and Eq. (15):

$$W_{a,cl} = \frac{1}{(1+W_{cl})} W_{cl} \quad (13)$$

$$W_{v,cl} = W_{cl} - W_{a,cl} \quad (14)$$

$$W_{cl} = \frac{M_v P_{v,cl}}{M_a P_{a,cl}} \quad (15)$$

Where M_v is the vapor molar mass, M_a is the air molar

mass, $P_{v,cl}$ and $P_{a,cl}$ are the vapor and air pressures of the cooler which are calculated from the following Eq. (16) and Eq. (17) respectively:

$$P_{v,cl} = \phi_{cl} P_{sat}(T_{cl}) \quad (16)$$

$$P_{a,cl} = P_{cl} - P_{v,cl} \quad (17)$$

Where P_{cl} is the pressure of the cooler equal to the pressure of the supply manifold, $P_{sat}(T_{cl})$ is the water saturation vapor pressure at the temperature of the cooler T_{cl} , and ϕ_{cl} is the relative humidity of the cooler.

The input pressure of the cathode $P_{ca,in}$ is calculated from the following Eq. (18), Eq. (19) and Eq. (20):

$$P_{ca,in} = P_{hm} \quad (18)$$

$$P_{hm} = P_{a,cl} + P_{v,hm} \quad (19)$$

$$P_{v,hm} = W_{cl} \frac{M_a}{M_v} P_{a,cl} = \frac{W_{v,hm}}{W_{a,cl}} \frac{M_a}{M_v} P_{a,cl} \quad (20)$$

Where P_{hm} is the pressure of the humidifier, M_v is the vapor molar mass, M_a is the air molar mass, $P_{a,cl}$ is the air pressure of the cooler, $P_{v,hm}$ is the vapor pressure of the humidifier, $W_{a,cl}$ is the air flow rate of the cooler, $W_{v,hm}$ is the vapor flow rate of the humidifier.

The relative humidity of the humidifier can be deduced directly from the previous formula Eq. (21):

$$\phi_{hm} = \frac{P_{v,hm}}{P_{sat}(T_{hm})} = \frac{P_{v,hm}}{P_{sat}(T_{cl})} \quad (21)$$

With $P_{v,hm}$ the vapor pressure of the humidifier, $P_{sat}(T_{hm})$ the saturation vapor pressure at the humidifier temperature and $P_{sat}(T_{cl})$ the saturation vapor pressure at the cooler temperature.

ii. At the anode

The humidifier of the hydrogen system is modelled to maintain the desired relative humidity level. The pressure $P_{an,in}$ as well as the flow rate $W_{an,in}$ at the anode inlet are calculated as follows in Eq. (22) and Eq. (23) respectively:

$$P_{an,in} = P_{H_2} + P_{v,inj} \quad (22)$$

$$W_{an,in} = W_{hm} = W_{H_2} + W_{v,inj} \quad (23)$$

Where $P_{v,inj}$ is the injected vapor pressure, P_{H_2} the anode hydrogen pressure, W_{H_2} the hydrogen flow rate and $W_{v,inj}$ is the injected vapor flow rate.

The vapor flow rate to be injected is calculated using a PI controller to control the relative humidity of the anode.

3. Results and discussions

Simulation was performed under the same conditions as before

with the relative humidity set for the anode and the cathode at 0.8. The relative humidity (RH) of the anode and the cathode is shown in Figure 8. Both relative humidities follows their respective targets perfectly. On the anode side (Figure 8b), water is continuously injected to keep the relative humidity at the desired level, compensate for the water drained by the electro-osmosis phenomenon and prevent the membrane from drying out. The amount of injected water, determined by the regulator, is shown in Figure 9.

For the cathode side (Figure 8a), a given amount of water is evacuated to avoid a membrane flooding. The amount of water evacuated, determined by the regulator, is shown in Figure 10. The test was also performed using Worldwide Light Vehicles Test Procedures (WLTP) cycle and the results obtained were in congruence to those with proper regulation.

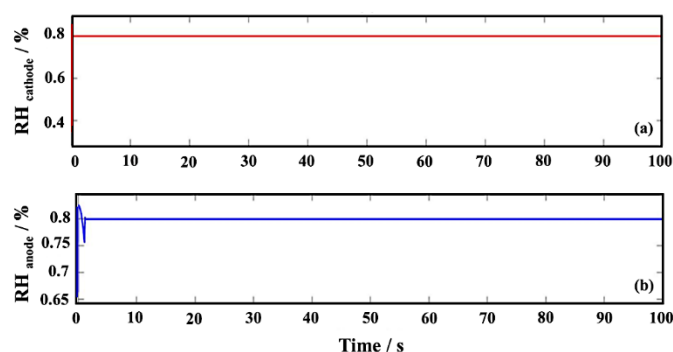


Fig. 8. Relative humidity in the cathode (a) and in the anode (b) for a current ramp from 0 to 300 A.

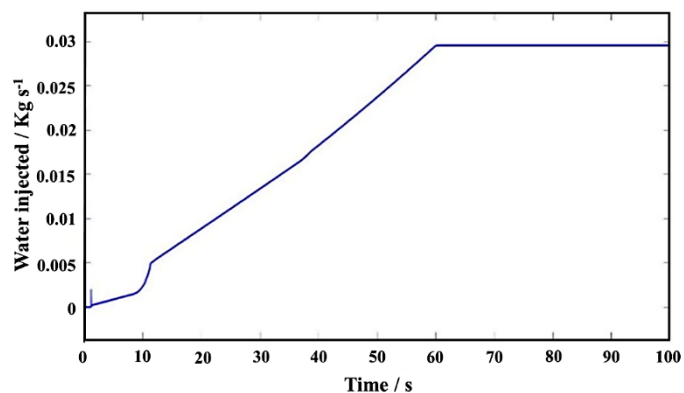


Fig. 9. Flow rate of water injected to regulate the relative humidity in the anode for a current ramp from 0 to 300 A.

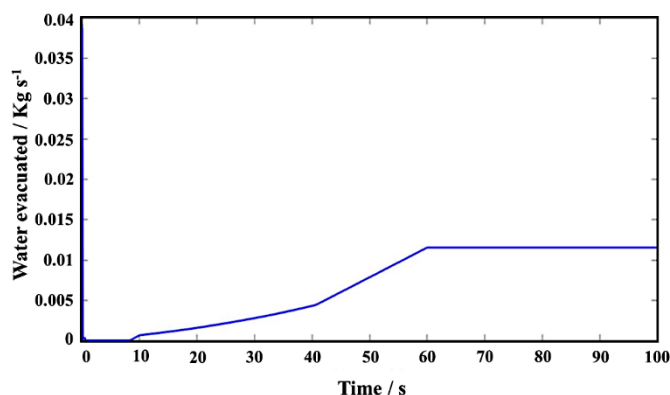


Fig. 10. Flow rate of water evacuated to regulate the relative humidity in the cathode for a current ramp from 0 to 300 A obtained by simulation.

3.1. Problem of carbon monoxide poisoning and its control strategy

Since the cost of producing hydrogen by clean electrolysis is too high, hydrogen is usually obtained by reforming natural gas according to the Eq. (24), or hydrocarbons.



The process produces a few pollutants, mainly CO_2 and CO . Carbon monoxide is considered an inhibiting compound for the FC and can cause critical performance losses. A study of Wilson et al. [16] showed that when the hydrogen used in the FC contained 5 ppm of CO , a 50 % reduction of the maximum power density was observed. This is due to the strong atomic bonds forming between the CO and the Pt catalyst support. The accumulation of carbon monoxide at the catalytic sites leads to a decrease in proton production causing a performances degradation of the FC system [20–23].

Studies have been carried out to find an alternative catalyst that would be more tolerant to contamination or a potential catalyst regeneration solution. These include the use of the Pt/Ru catalyst, which is considered the most CO resistant alternative potential catalyst because the $Ru-CO$ bond is stronger than the $Pt-CO$ one [24]. Therefore, CO preferentially binds to Ru instead of Pt , allowing the Pt active sites to remain available for the hydrogen.

Increasing the stack operating temperature can also be considered as a solution in order to limit poisoning, but a membrane able to withstand high temperatures is required [25–27]. The current chosen solution is "air-bleeding", which consists of injecting oxygen into the anode so that it can react with CO and release it from the catalytic Pt sites [28–31].

3.1.1. Model of activation voltage

In a FC, there are three voltage drops: the ohmic voltage drop, the concentration voltage drops, and the activation voltage drop. The activation voltage was modelled which is a voltage drop defined by the potential difference above the equilibrium potential required to overcome the activation energy to produce a requested

current. It is calculated by the following Eq. (25):

$$V_{act} = \frac{RT}{\alpha n F} \ln\left(\frac{j}{j_0}\right) \quad (25)$$

Where R is the ideal gas constant, α is the load transfer coefficient, n is the number of electrons exchanged, F is the Faraday's constant (96485.33 A.s.mol⁻¹), j_0 is the current density at equilibrium (A.cm⁻²), T is the temperature (°C) and j is the current density (A.cm⁻²).

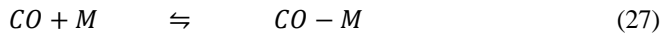
3.1.2. Model of anode poisoning

During poisoning, the equilibrium current density varies as a function of the carbon monoxide recovery rate θ_{CO} according to the following Eq. (26) [32]:

$$j_0 = j_{0,se}(1 - \theta_{CO})^2 \quad (26)$$

Where $j_{0,se}$ is the current density without poisoning.

The phenomenon of poisoning occurring at the active surface on the electrodes was also modelled. It leads to the occupation of Pt catalytic sites by carbon monoxide molecules, as described in the Eq. (27). This phenomenon causes an increase of the activation voltage and thus a voltage drop [30–32] of the FC.



- i. Calculation of hydrogen recovery rate on the active surface (Theta H or θ_H).

The hydrogen recovery rate on the active surface, meaning the ratio of platinum surface occupied by hydrogen on the anode side, is determined.

The calculation is performed using the following Eq. (28) [33]:

$$\rho \frac{d\theta_H}{dt} = 2k_{ads}^H C_{H,e} \theta_M^2 - b_{ads}^H k_{ads}^H \theta_H^2 - 2k_{ox}^H O_H \left(e^{\frac{\alpha_a F \eta_c}{RT}} - e^{-\frac{\alpha_c F \eta_c}{RT}} \right) - 2k_{ox}^{H-0} \theta_O \theta_H^2 \quad (28)$$

Where:

- $q_{H,ads} = 2k_{ads}^H C_{H,e} \theta_M^2 - b_{ads}^H k_{ads}^H \theta_H^2$ is the reaction rate of the adsorbed hydrogen.
 - $q_{H,ox} = 2k_{ox}^H O_H \left(e^{\frac{\alpha_a F \eta_c}{RT}} - e^{-\frac{\alpha_c F \eta_c}{RT}} \right)$ is the reaction rate of the electro-oxidation of the adsorbed hydrogen.
 - $q_{H-0,ox} = 2k_{ox}^{H-0} \theta_O \theta_H^2$ is the reaction rate of the heterogeneous oxidation of hydrogen.
 - k_i^j and b_i^j are the kinetic constants of the corresponding chemical reactions.
- ii. Calculation of carbon monoxide recovery rate on the active surface (Theta CO or θ_{CO}).

The carbon monoxide recovery rate on the active surface, i.e.

ratio of platinum surface occupied by carbon monoxide on the anode side, is determined by the following Eq. (29):

$$\rho \frac{d\theta_{CO}}{dt} = k_{ads}^{CO} C_{CO,e} \theta_M e^{-\frac{\beta r \theta_{CO}}{RT}} - b_{ads}^{CO} k_{ads}^{CO} O_{CO} e^{\frac{(1-\beta)r \theta_{CO}}{RT}} - 2k_{ox}^{CO} O_{CO} \sinh\left(\frac{F \eta_a}{2RT}\right) - k_{ox}^{C-0} \theta_O \theta_{CO} \quad (29)$$

Where:

- $q_{CO,ads} = k_{ads}^{CO} C_{CO,e} \theta_M e^{-\frac{\beta r \theta_{CO}}{RT}} - b_{ads}^{CO} k_{ads}^{CO} O_{CO} e^{\frac{(1-\beta)r \theta_{CO}}{RT}}$ is the reaction rate of the adsorbed carbon monoxide.
 - $q_{CO,ox} = 2k_{ox}^{CO} O_{CO} \sinh\left(\frac{F \eta_a}{2RT}\right)$ is the reaction rate of the electro-oxidation of the adsorbed carbon monoxide.
 - $q_{CO-0,ox} = k_{ox}^{C-0} \theta_O \theta_{CO}$ is the reaction rate of the heterogeneous oxidation of carbon monoxide.
- iii. Calculation of oxygen recovery rate on the active surface (Theta O or θ_O).

The oxygen recovery rate on the active surface, i.e. ratio of platinum surface occupied by oxygen on the anode side, is determined by the following Eq. (30):

$$\rho \frac{d\theta_O}{dt} = 2k_{ads}^O C_{O,e} \theta_M^2 - b_{ads}^O k_{ads}^O \theta_O^2 - k_{ox}^{H-0} \theta_O \theta_H^2 - k_{ox}^{C-0} \theta_O \theta_{CO} \quad (30)$$

Where:

- $q_{O,ads} = 2k_{ads}^O C_{O,e} \theta_M^2 - b_{ads}^O k_{ads}^O \theta_O^2$ is the reaction rate of the adsorbed oxygen.
- $q_{H-0,ox} = k_{ox}^{H-0} \theta_O \theta_H^2$ is the reaction rate of the heterogeneous oxidation of hydrogen.
- $q_{CO-0,ox} = k_{ox}^{C-0} \theta_O \theta_{CO}$ is the reaction rate of the heterogeneous oxidation of carbon monoxide.

- iv. Calculation of platinum recovery rate (Theta M or θ_M).

The platinum recovery rate is determined in relation with the total theoretically available platinum surface.

The calculation is carried out using the following Eq. (31):

$$\theta_M = 1 - \theta_H - \theta_O - \theta_{CO} \quad (31)$$

In order to evaluate the impact of this phenomenon on the performance of the FC, several simulations for poisoning levels ranging from 0 ppm CO to 100 ppm were carried out. The results obtained with a 3 A.s⁻¹ ramp are illustrated in Figure 11.

Since the system was in equilibrium at the beginning of the simulation, the effect of the CO concentration at the anode on the FC voltage and on the activation voltage were studied. The evolution of the FC voltage and the activation voltage are shown in Figure 11a and Figure 11b respectively. On the Figure 11b, it is shown that the higher the poisoning level, the higher the activation voltage. This means that it is necessary to supply more energy to carry out the reaction, resulting in greater voltage drops, as shown in Figure 11a. The simulation for the poisoning was carried out only for a constant current of 100 A and a poisoning level corresponding to 100 ppm CO. The H₂ and CO recovery rates and the FC voltage resulting from this poisoning are shown in Figure 12 and Figure 13 respectively. It was observed that the CO recovery rate starts to increase at the expense of the hydrogen recovery rate. Since the CO-Pt bond is stronger than the H-Pt bond, CO molecules tend to create a bond with platinum, driving the hydrogen away from the active surface and taking its place on the Pt active sites. This prevents the catalysis of the hydrogen dissociation reaction into H⁺ ions, explaining the voltage drop observed in Figure 13.

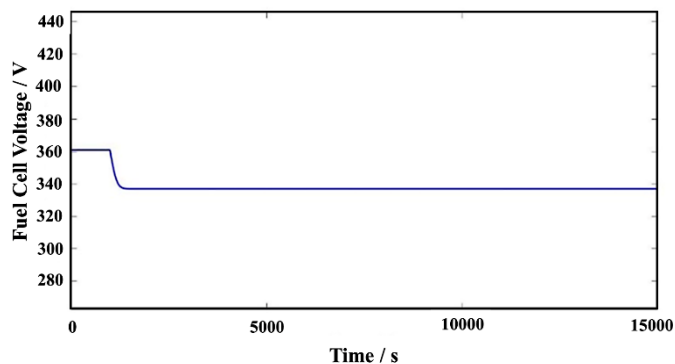


Fig. 13. FC voltage for a 100 ppm CO poisoning (I=100 A) obtained by simulation.

iv. Strategy adopted: air bleeding

The proposed solution is to inject a given amount of air (air-bleeding) depending on the H₂ flow rate. The injected air reacts with CO according to the previous Eq. (30) [34,35].

The same conditions as the previous simulation were used: a constant current of 100 A and a poisoning level of 100 ppm CO. The evolution of the hydrogen, carbon monoxide and oxygen recovery rates are shown in Figure 14. The evolution of the FC voltage is shown in Figure 15. At t=1000 s, marking the beginning of the poisoning, the results are similar to the previous simulation since the conditions are unchanged. At t=5000 s, the injection of oxygen into the anode is started. The injected oxygen represents 5% of the hydrogen mass flow. Generally, it does not exceed 10%-13% to remain below the explosive limit of H₂. The oxygen recovery rate increases, as oxygen is injected, and then returns to zero. This proves that the oxygen particles are no longer in contact with the platinum and have formed a bond with the carbon monoxide to form CO₂. Indeed, afterwards, the CO recovery rate begins to decrease, showing that the reaction of CO with O₂ begins, in favor of the hydrogen recovery rate. As shown in Figure 15, when the poisoning begins, the FC voltage decreases from 360 V down to 340 V and reaches a plateau when the recovery rates become constant. As soon as oxygen is injected and that the carbon monoxide recovery rate starts to decrease, the exchange current density of the FC starts to increase, resulting in a decrease of the activation voltage and an increase of the FC voltage back up to 360 V. So, the regeneration strategy developed allows the recovery of the voltage and of the initial performances of the FC, as shown in Figure 15.

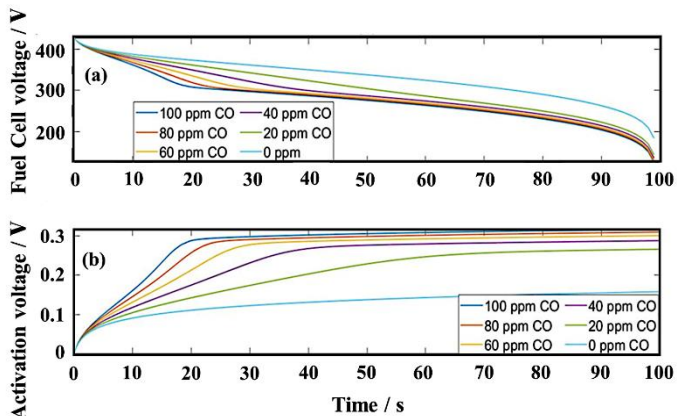


Fig. 11. FC voltage (a) and activation voltage (b) for different poisoning levels obtained by simulation (I=3 A/s).

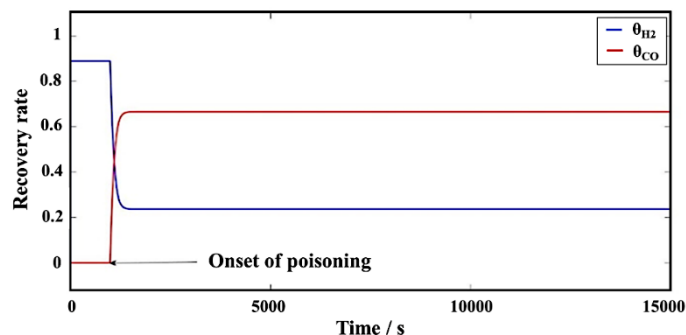


Fig. 12. H₂ (blue line) and CO (orange line) recovery rates for a 100 ppm CO poisoning (I=100 A) obtained by simulation.

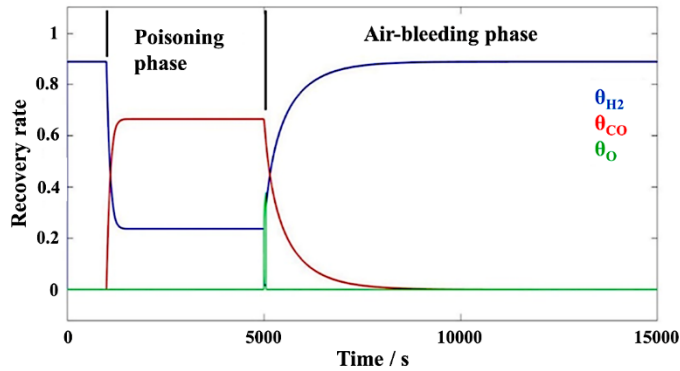


Fig. 14. H₂, CO and O₂ recovery rates for a 100 ppm CO poisoning and a 5% O₂ injection (I=100 A) obtained by simulation.

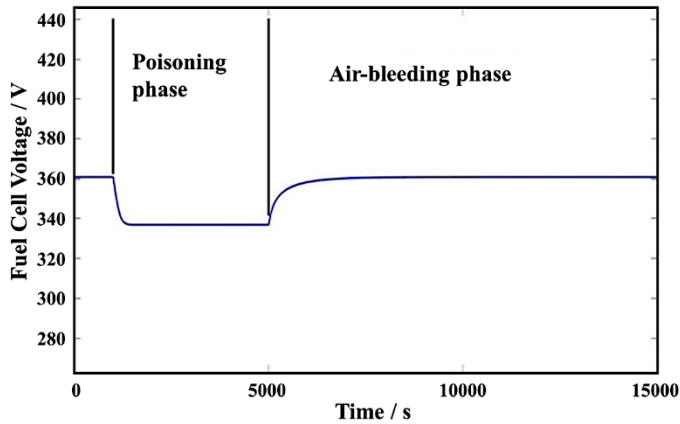


Fig. 15. FC voltage for a 100 ppm CO poisoning and a 5% O₂ injection (I=100 A) obtained by simulation.

3.1.3. Study of the cold start problem and strategy adopted

One of the main drawbacks of the FC is its response time of about 10 s which affects vehicle dynamic performance during strong accelerations. Therefore, a high-power rating is required and consequently an optimal and efficient cooling as well. With a relatively high operating temperature (80°C), starting the FC at negative temperatures is delicate. It generally requires several minutes in usual conditions. Therefore, it is interesting to study the problem of cold start and propose strategies to facilitate it.

The oxidation-reduction reaction taking place within the FC is exothermic, with water being produced. Its operation induces an increase in the quantity of heat released, but also of water produced, the starting procedures (current profiles, stoichiometry) are more complex, and water becomes an obstacle to FC starting at negative temperature.

Autonomous starting of the FC (without external energy supply)

at a critical temperature below 3°C is a fundamental constraint. Indeed, the solidification of the water contained in the active layers and in the gas diffusion layer (GDL) hinders the catalytic sites and prevents the diffusion of gases. Purges are carried out after system shutdown to remove some of the water stored by the membranes in order to limit damage of the FC and create storage capacity for the water produced at start-up. In addition, the thickness of the membrane can play an important role. The thinner the membrane, the faster the ice it contains melts, and the lesser water accumulates [36].

The condition and performance of the FC is directly affected by the possible formation of ice:

- i. It reduces the power delivered by the FC by blocking the electrochemical sites.
- ii. The conductivity of the diaphragm drops, causing major degradation in the voltage delivered by the battery.
- iii. It mechanically damages the membrane if it swells.

The cold start phenomenon and its consequences on the FC are summed up in Figure 16.

The model developed consists of a FC, a battery, and a heat exchanger, as shown in Figure 17. The heat transfer is performed thanks to a mixture of water and glycol [37]. The maximum thermal power of the heat exchanger is 5 kW. In this part, only the thermal effect is considered.

The strategy adopted for the cold start problem is the following:

- i. If the FC temperature is negative ($T_{FC} < 0^{\circ}\text{C}$): the battery-powered heat exchanger is used to heat the stack until its temperature T_{FC} is equal to 0°C , and the ice begins to melt.
- ii. From $T_{FC} = 0^{\circ}\text{C}$: the heat released by the chemical reaction in the FC is used to increase the stack temperature until it reaches its nominal operating temperature ($T_{FCn} = 80^{\circ}\text{C}$).

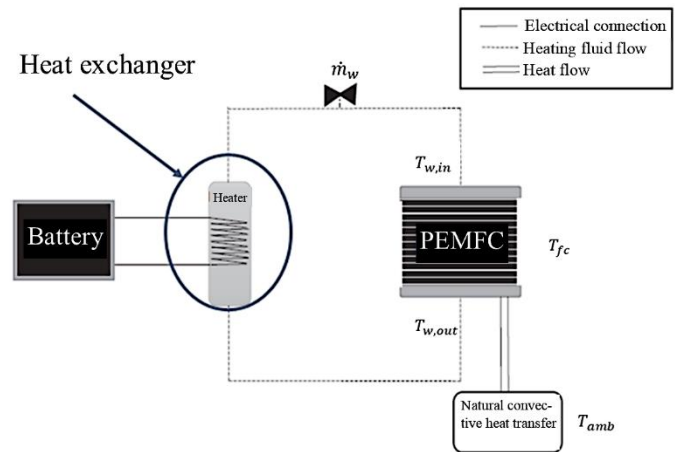


Fig. 16. Cold-Start phenomenon.

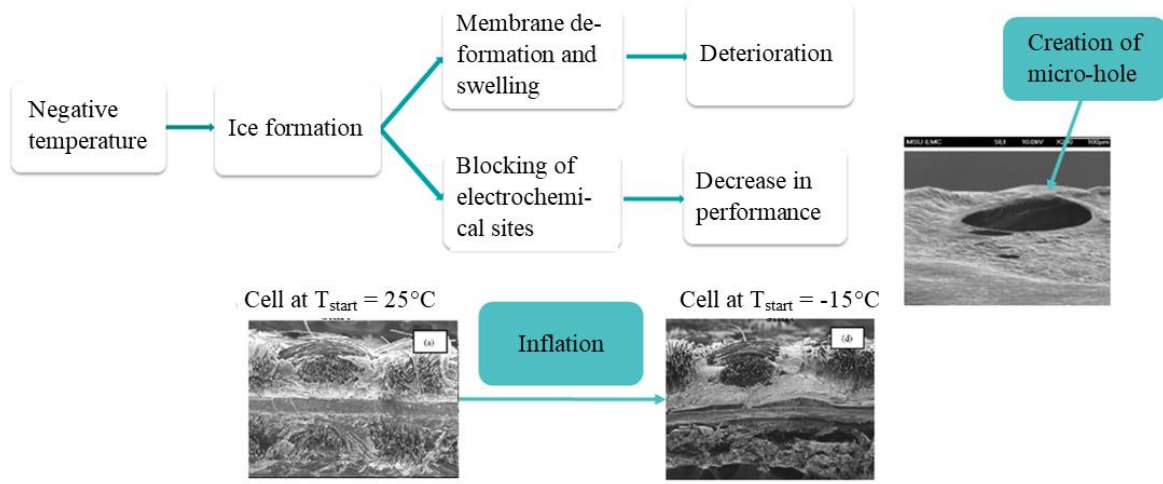


Fig. 17. Schematic diagram of the fuel cell heat exchanger and its power supply.

3.2. Model of radiator

The fluid temperature is defined by the following Eq. (32), Eq. (33), Eq. (34) and Eq. (35):

$$T_w = T_{w,init} + \frac{1}{m_w c_w} \int_0^t (\Delta S_{he} - \Delta S_w) T_w dt \quad (32)$$

$$\Delta S_{he} = \frac{R_w i_{ch}^2}{T_w} \quad (33)$$

$$\Delta S_w = \frac{K_w}{T_w} (T_w - T_{FC}) \quad (34)$$

$$K_w = \dot{m}_w c_w \left[1 - \exp\left(-\frac{h_{cw} S_{cw}}{\dot{m}_w c_w}\right) \right] \quad (35)$$

Where T_w is the fluid temperature, $T_{w,init}$ is the fluid initial temperature, m_w is the fluid mass, c_w is the fluid heat capacity, ΔS_w is the entropy or heat transferred to the heating fluid ($J.K^{-1}$), ΔS_{he} is the heat flux from the heating element ($J.K^{-1}$), R_w is the radiator thermal resistance, i_{ch} is the radiator current, T_{FC} is the FC temperature, \dot{m}_w is the fluid mass flow, h_{cw} is the coefficient of heat transfer by forced convection and S_{cw} is the heat transfer surface area.

The cold start strategy developed has been tested on the FC model. The temperature of the FC changes according to Eq. (35):

$$T_{FC} = T_{FC,init} + \frac{1}{(mC_P)_{FC}} \int_0^t (\Delta S_{w2} - \Delta S_{amb}) T_{FC} dt \quad (36)$$

With:

$$\Delta S_{w2} = \frac{K_w}{T_{FC}} (T_w - T_{FC}) \quad (36)$$

$$\Delta S_{amb} = \frac{h_{nc} S_{nc}}{T_{FC}} (T_{FC} - T_{amb}) \quad (37)$$

Where T_{FC} is the FC temperature $T_{FC,init}$ is the initial FC temperature, ΔS_{w2} is the entropy, ΔS_{amb} is the heat flux between the FC and the environment, T_w is the fluid temperature, T_{amb} is the room temperature, h_{nc} is the coefficient of heat transfer by natural convection, S_{nc} is the surface of walls of the FC.

The evolution of the ice fraction and the FC temperature are shown in Figure 18. The ambient temperature was set to $-20^\circ C$ and it was assumed that 90% of the membrane surface was frozen. At start-up, the stack temperature is equal to the room temperature. The evolution of the radiator fluid temperature during this cold start scenario is shown in Figure 19.

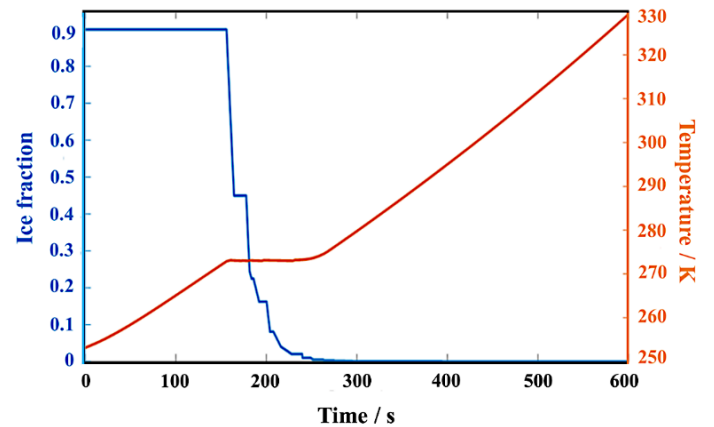


Fig. 18. Evolution of the stack temperature and the ice fraction in the membrane during the cold start obtained by the FC model for a room temperature of $-20^\circ C$.

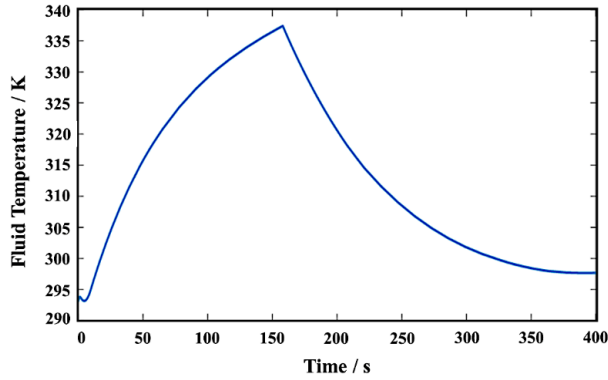


Fig. 19. Evolution of the radiator fluid temperature during the cold-start obtained by the FC model for a room temperature of -20°C .

The heat exchanger is powered by the battery, the temperature of the fluid rises and heats the FC up to $t = 150$ s, as shown in Figure 19, where the stack temperature reaches 0°C (Figure 18). After 150 s, the heat exchanger is switched off and the temperature of the fluid begins to drop, as shown in Figure 19. Up to $t = 150$ s, the FC temperature increases from -20°C to 0°C , which corresponds to the operating time of the exchanger, while the ice fraction remains constant. Once the stack temperature reaches 0°C , it takes 1 min to melt. The temperature remains constant at 0°C during this phase. Once all the ice has melted and the ice fraction is down to zero, the stack temperature continues to increase until it reaches its nominal value.

It is assumed that if the outside temperature is negative, there is formation of ice, so a part of the surface of the membrane is no longer active. Therefore, it is necessary to know the evolution of the active surface depending on the ice fraction. It is assumed that if $T_{\text{FC}} < 0^{\circ}\text{C}$, 90% of the membrane is frozen. The initial ice fraction can be modified in the Matlab script. If the stack temperature is positive ($T_{\text{FC}} > 0^{\circ}\text{C}$), the active surface of the membrane is equal to its total surface ($S_{\text{act}} = S_{\text{total}}$). Otherwise, only the part of the membrane, that is not covered with ice, is active, as stated in the following equations Eq. (39), Eq. (40), Eq. (41) and Eq. (42):

$$S_{\text{act}} = S_{\text{total}}(1 - f) \quad (39)$$

$$f = \frac{v_{\text{ice}}(t)}{v_{\text{vide}}} \quad (40)$$

$$v_{\text{ice}}(t) = \frac{m_{\text{ice}}(t)}{\rho_{\text{ice}}} \quad (41)$$

$$m_{\text{ice}}(t) = m_{\text{ice}}(t - 1) - \frac{1}{L_{\text{ice-water}}} \int \dot{Q}_{\text{ice}} \quad (42)$$

f is the ice fraction, ρ_{ice} is the ice density equals to $900 \text{ kg}\cdot\text{m}^{-3}$, m_{ice} is the ice mass (kg), and v_{ice} is the ice volume (m^3).

The evolution of the membrane active surface during the cold start scenario is shown in Figure 20. From 0 to 150 s, the membrane active surface is stable at only about 10% of the total surface, as shown in Figure 20, until the stack temperature reaches 0°C at 150 s and the ice starts melting. From 150 to 240s, the ice fraction

decreases, diminishing the membrane surface covered with ice and increasing the membrane active surface until all the ice disappears and the entire surface of the membrane can be used.

The supervisor's role is to determine the references of the different control loops (control of the air system, cathode outlet valve, stack set point current, etc.) according to the current required from the FC and its operating conditions (stack temperature, cathode, and anode pressure). The stack reference current is calculated at the local supervisor level according to the load and the state of the FC. If the temperature is negative, there will be a formation of ice and therefore a decrease of the number of active sites.

A strategy for determining the reference current has been adopted to protect the FC during cold start:

- i. If $T_{\text{FC}} < 0^{\circ}\text{C}$, then $I_{\text{FC}} = 0$: the current of the FC is zero until the ice starts melting at $T_{\text{FC}} = 0^{\circ}\text{C}$.
- ii. If $0^{\circ}\text{C} \leq T_{\text{FC}} \leq 5^{\circ}\text{C}$ and $I_{\text{load}} < I_{\text{FC,max}}/2$, then $I_{\text{FC}} = I_{\text{load}}$: the FC can supply power as long as the current demanded is not too high.
- iii. If $0^{\circ}\text{C} \leq T_{\text{FC}} \leq 5^{\circ}\text{C}$ and $I_{\text{load}} \geq I_{\text{FC,max}}/2$, then $I_{\text{FC}} = I_{\text{FC,max}}/2$: the power supplied by the FC is limited to 50% of its maximum power.
- iv. If $T_{\text{FC}} > 5^{\circ}\text{C}$, then $I_{\text{FC}} = I_{\text{load}}$: it is assumed that all the ice has melted. Therefore, the full power of the FC can be used.

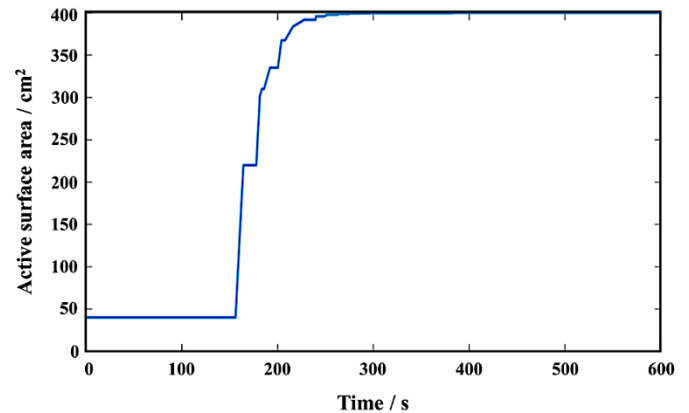


Fig. 20. Evolution of the active surface of the membrane during the cold start obtained by the FC model for a room temperature of -20°C .

4. Conclusion

This study focused on the simulation of the FC operation and performances degradations. The FC modelling was first described. The content of the model and the method used to create it were detailed. The different parts of the model, i.e. the cathode where the air is brought into the cell, the anode, where the hydrogen is provided and the membrane, where the water transport phenomena take place, were modelled. The model was then able to accurately simulate the FC operation. Performance degradation factors were systematically examined, commencing with water management.

The model not only incorporated the influence of water on cell performance but also accounted for degradation phenomena such

as anode desiccation and cathode flooding. To mitigate these issues, a humidity regulation system employing proportional-integral (PI) regulators was proposed, maintaining optimal humidity levels at the membrane.

The study delved into the challenge of anode poisoning resulting from carbon monoxide, a byproduct of natural gas reforming. To address this concern, an "air-bleeding" strategy was meticulously explored and elucidated. Lastly, the impact of cold start scenarios on FC performance was scrutinized, leading to the proposal of a thermal management strategy to facilitate FC operation under adverse ambient temperatures.

In conclusion, the developed model not only enables accurate FC behavior simulation but also accommodates specific scenarios that impede FC performance, offering innovative solutions to mitigate their impacts on FC operations.

Acknowledgment

This work was carried out at Altran Prototypes Automobiles (APA) as a part of the Hybrid Innovative Powertrain (HIP) project within the Capgemini Engineering Research and Innovation Department. The authors would like to thank Damien Clemencon and Imen Aribi for their contribution to the work.

Credit Author Statement

Fatima Haidar: Writing-original draft, writing-review & editing, validation. **Divyesh Arora:** Writing-original draft, conceptualization, data curation, formal analysis. **Adrien Soloy:** review & editing. **Thomas Bartoli:** Review & editing.

References

- Jemei S. Ph.D. Thesis, Belfort Technology and Franche Comte University, France. 2004.
- Apostolou D, Xydis G. Renewable and Sustainable Energy Reviews 2019;113. <https://doi.org/10.1016/j.rser.2019.109292>.
- Eberle U, Müller B, von Helmolt R. Energy and Environmental Science 2012;5:8780–98. <https://doi.org/10.1039/c2ee22596d>.
- Haddad A. Ph.D. Thesis, Belfort Montbeliard University, France. 2011.
- Kocakulak T, Arslan A. Investigation of the Use of Fuel Cell Hybrid Systems for Different Purposes. Engineering Perspective 2023; 3:1–8.
- Boyacıoğlu NM, Kocakulak T, Batar M, Uyumaz A, Solmaz H. Modelling and Control of a PEM Fuel Cell Hybrid Energy System Used in a Vehicle with Fuzzy Logic Method. International Journal of Automotive Science and Technology 2023; 7:295–308. <https://doi.org/10.30939/ijastech..1340339>.
- Cavaliere S, Zatoń M, Farina F, Jones D, Rozière J. Chapter 9: Electrospun Materials for Proton Exchange Membrane Fuel Cells and Water Electrolysis. RSC Soft Matter, vol. 2018- January 2018. <https://doi.org/10.1039/9781788012942-00205>.
- Haidar F. Ph.D. Thesis, Montpellier University, France. Montpellier, 2018.
- Le Ny M. Ph.D. Thesis, Grenoble University, France. 2012.
- Fouquet N, Doulet C, Nouillant C, Dauphin-Tanguy G, Ould-Bouamama B. J. of Power Sources 2006;159:905–13. <https://doi.org/10.1016/j.jpowsour.2005.11.035>.
- Jimenez-Morales I, Haidar F, Cavaliere S, Jones D, Rozière J. Strong Interaction between Platinum Nanoparticles and Tantalum-Doped Tin Oxide Nanofibers and Its Activation and Stabilization Effects for Oxygen Reduction Reaction. ACS Catal 2020; 10:10399–411. <https://doi.org/10.1021/acscatal.0c02220>.
- Zawodzinski TA, Derouin C, Radzinski S, Sherman RJ, Smith VT, Springer TE, et al. J. of the Electrochemical Society 1993;140:3278.
- Amphlett JC, Baumert RM, Mann RF, Peppley BA, Roberge PR, Harris TJ. J. of the Electrochemical Society 1995;142.
- Springer TE, Zawodzinski TA, Gottesfeld S. J. of the Electrochemical Society 1991;138:208.
- Ramousse J, Deseure J, Lottin O, Didierjean S, Maillet D. J. of Power Sources 2005;145:416–27. <https://doi.org/10.1016/j.jpowsour.2005.01.067>.
- Wilson MS, Derouin CR, Valerio JA, Gottesfeld S. Proc. 28th Intersociety Energy Conversion Engineering conference, Atlanta, Georgia, 1993.
- Dicks AL, Rand DAJ. Fuel Cell Systems Explained, WILEY,Griffith University- Brisbane, Australia and CSIRO Energy-Melbourne, Australia. 2018.
- Dutta S, Shimpalee S, van Zee JW. International Journal of Heat and Mass Transfer 2001.
- Pukrushpan JT. Ph.D. Thesis, Michigan University, United states. 2003.
- Ciureanu M, Wang H. Electrochemical impedance study of anode CO-poisoning in PEM fuel cells. Journal of New Materials for Electrochemical Systems 2000;3.
- Tingelöf T, Hedström L, Holmström N, Alvfors P, Lindbergh G. International Journal of Hydrogen Energy 2008;33:2064–72. <https://doi.org/10.1016/j.ijhydene.2008.02.002>.
- De Beccdelièvre AM, de Beccdelièvre J, Clavilier J. J. Electroanal. Chem 1990; 294:97–110.
- Kim J-D, Park Y-I, Kobayashi K, Nagai M. J. of Power Sources 2001;127.
- Urian RC, Gullá AF, Mukerjee S. J. of Electroanalytical Chemistry 2003;554–555:307–24. [https://doi.org/10.1016/S0022-0728\(03\)00241-9](https://doi.org/10.1016/S0022-0728(03)00241-9).
- Wee JH, Lee KY. J. of Power Sources 2006;157:128–35. <https://doi.org/10.1016/j.jpowsour.2005.08.010>.
- Murthy M, Esayian M, Lee W, van Zee JW. J. of The Electrochemical Society 2003;150:A29. <https://doi.org/10.1149/1.1522383>.
- Kawatsu S. Canada Patent,CA 2214769A1. 5,925,476, 1999.
- Springer TE, Rockward T, Zawodzinski TA, Gottesfeld S. J. of The Electrochemical Society 2001;148:11–23.
- Carrette LPL, Friedrich KA, Huber M, Stimming U. Physical Chemistry Chemical Physics 2001;3:320–4. <https://doi.org/10.1039/b005843m>.
- Baschuk JJ, Li X. International Journal of Energy Research 2003;27:1095–116. <https://doi.org/10.1002/er.934>.
- Zamel N, Li X. International Journal of Hydrogen Energy 2008;33:1335–44. <https://doi.org/10.1016/j.ijhydene.2007.12.060>.
- James McBreen, Sanjeev Mukerjee, S. Srinivasan. Electrochemical Society, Pennington, New Jersey. vol. 1. 1997.
- Baschuk JJ, Li X. International Journal of Energy Research 2003;27:1095–116. <https://doi.org/10.1002/er.934>.
- Shah AA, Sui PC, Kim GS, Ye S. J. of Power Sources 2007;166:1–21. <https://doi.org/10.1016/j.jpowsour.2007.01.020>.
- Delgado S, Lagarteira T, Mendes A. Air bleeding strategies to increase the efficiency of proton exchange membrane fuel cell stationary applications fuelled with CO ppm-levels. Int J Electrochem Sci 2020; 15:613–27. <https://doi.org/10.20964/2020.01.58>.
- Luo Y, Jiao K. Progress in Energy and Combustion Science 2018;64:29–61. <https://doi.org/10.1016/j.peccs.2017.10.003>.
- Amamou AA, Kelouwani S, Boulon L, Agbossou K. IEEE Access 2016;4:4989–5002. <https://doi.org/10.1109/access.2016.2597058>.